Van-der-Waals based Solvates of C_{60} with CBr_2Cl_2 and $CBr_2(CH_3)_2$

Jin Ye[1], Maria Barrio[1], René Céolin[1,2], Navid Qureshi[3], Ivo B. Rietveld[4], Josep Lluís Tamarit[1,*]

[1]Departament de Física, ETSEIB, Universitat Politècnica de Catalunya, Diagonal 647, 08028 Barcelona, Catalonia, Spain

[2] LETIAM, EA7357, IUT Orsay, Université Paris Sud, rue Noetzlin, 91405 Orsay Cedex, France

[3] Institut Laue Langevin, 71 avenue des Martyrs - CS 20156 - 38042 GRENOBLE CEDEX 9, France

[4] Laboratoire de Chimie Physique, CAMMAT, Faculté de Pharmacie, Université Paris Descartes, 4 avenue de l'Observatoire, 75006 Paris, France

* Corresponding author: J.Ll. Tamarit, e-mail: josep.lluis.tamarit@upc.edu

Phone: +34 93 401 65 64

Abstract

We demonstrate that solvates of fullerene C_{60} form very predictable structures with finely tunable properties through the choice of the second component or solvent. Cubic co-crystals of $C_{60}\cdot 12CCl_2Br_2$ and $C_{60}\cdot 12CBr_2(CH_3)_2$ were grown at room temperature in saturated solutions of fcc C_{60} and the respective solvents (with C_{2v} molecular symmetry) They are unstable in air and transform spontaneously into the hexagonal co-crystals $C_{60}\cdot 2CCl_2Br_2$ or $C_{60}\cdot 2CBr_2(CH_3)_2$. Whereas, the cubic co-crystals have positive excess volumes (+2% and +5%, respectively), the stable hexagonal crystals, for which structures are given for the first time, possess negative excess volumes (-5% and -4.3%, respectively). The unit-cell volumes for both cubic and hexagonal co-crystals depend exclusively on the van-der-Waals volumes of the constituents and this correlation has been confirmed using previously published data.

1. Introduction

The face-centered cubic (fcc) structure of fullerene C_{60} has a unique closed-cage structure and often forms solvates by incorporating solvent molecules into a host structure governed by C_{60}. Production, purification, and also functionalization of fullerenes involve their dissolution in solvents with simple molecular structures. The formation of solvates may interfere with these processes, because they have the tendency to reach saturation at lower concentrations than fcc C_{60}. Solvates commonly exhibit incongruent melting giving rise to fcc C_{60} and its saturated solution. Only above the incongruent melting temperature does the saturated solution reflect the solubility of fcc C_{60}, whereas below this temperature the solubility of its solvate will be obtained [1-7].That these fundamental phenomena [8-12]. are linked to practical issues is demonstrated by one of the most typical fullerene derivatives used in photovoltaic cells, [6,6]-phenyl C61 butyric acid methyl ester (PCBM), an electron-acceptor fullerene derivative, for which the solar cell efficiency strongly depends on the difference in molecular packing with toluene, chlorobenzene, or dichlorobenzene [13,14]. It is therefore obvious that the stability and composition of fullerene solvates have been the focus of a large number of studies [15-21].

A large number of fullerene solvates containing aromatic solvents has been studied, see for example the review of Korobovet al. [18]. This compilation reveals that solvate structures are “typical van-der-Waals complexes”, with small negative excess volumes and high packing coefficients (between 0.72 and 0.78). In C_{60} solvates containing tetrahedral molecules with stoichiometry 1:2, such as $C_{60}\cdot 2YCCl_3$ (Y = H, CH_3, Br, Cl) and $C_{60}\cdot 2HCBr_3$, previous results have demonstrated that the van-der-Waals volume of the solvent molecules has a proportional relationship with the unit-cell volume of the solvates. However, the external atoms on highly symmetrical solvent molecules appear to be less important, at least within the considered temperature ranges [22]. For example, solvates containing the solvent molecules chloroform, $HCCl_3$, and bromoform, $HCBr_3$, with molecular symmetry C_{3v} possess a hexagonal crystal symmetry (space-group P6/mmm) in which the C_{60} and the haloform molecules are stacked in alternating layers (the [001] hexagonal planes) [23]. For solvates containing the solvent molecules $(CH_3)CCl_3$ and $BrCCl_3$ with the same C_{3v} symmetry or CCl_4 with the higher molecular symmetry Td, similar results were found for the solvate’s crystal symmetry and for its crystal lattice anisotropy [24-28].

The packing in the two groups of solvates is determined by different weak intermolecular interactions, however, induced polarization of C_{60} may play a more important

role in the solvates $C_{60}\cdot 2HCCl_3$ and $C_{60}\cdot 2HCBr_3$ [23,29] than in solvates containing $(CH_3)CCl_3$, $BrCCl_3$, and CCl_4 due to the lower dipole moment of these solvent molecules, which in addition show a noticeable lower packing coefficient [22,24,25] than $C_{60}\cdot 2HCCl_3$ and $C_{60}\cdot 2HCBr_3$ [23,29] solvates. Because of the low number of solvates studied so far, the overall trends remain tentative and more data on the physical properties of other C_{60} solvates related to lattice symmetry and packing will be necessary to improve our understanding of these systems.

In this work solvates of C_{60} with two brominated polar solvents $CBr_2(CH_3)_2$ and CBr_2Cl_2 are described. The aim is two-fold. Firstly, it is well known that C_{60} forms stable co-crystals with bromoform ($HCBr_3$) that possesses considerable orientational disorder in the co-crystals. Thus, comparison with different brominated polar solvents can shed light onto the stability and other properties of these solvates. Secondly, the crystallographic packing and the crystal anisotropy of the solvates will be explained on the basis of the van-der-Waals volume of the constituents and a general relationship will be proposed.

2. **Experimental Section**

Fullerene C_{60} was purchased from TermUSA (purity > 99.98%). 2,2-dibromo-propane ($CBr_2(CH_3)_2$) was purchased from Aldrich with a purity of 95% and was fractionally distilled. The purified compound showed a melting temperature (255.0 K) in agreement with the literature [30]. Dibromo-dichloro-methane(CBr_2Cl_2) was purchased from Across with a purity of 98% and was used without further purification.

Solvates were prepared at room temperature by mixing fcc C_{60} crystals and $CBr_2(CH_3)_2$ or CBr_2Cl_2 solvents in screw-cap tubes. The heterogeneous mixtures were stored for several months in the absence of light and they were periodically monitored by optical microscopy. After about 2 weeks, the fcc C_{60} crystals started disappearing and new crystals with a different morphology appeared, which has been confirmed by scanning electron microscopy (SEM, a JEOL-7100F, scanning voltage20 kV).

Differential scanning calorimetry (DSC) experiments were performed on a Q100 analyzer from TA Instruments (New Castle, DE, USA) with masses from 10 to 50 mg and heating rates from 0.2 up to 2 K min^{-1} were used. The measurements were carried out on samples in hermetically sealed high-pressure stainless steel pans from Perkin–Elmer to resist the vapor pressures of the solvents.

Thermogravimetry (TG) experiments were conducted at a 2 K min^{-1} rate under a nitrogen flow with a Q50 thermobalance from TA Instruments (New Castle, DE, USA). The initial sample masses ranged between 2 and 10 mg.

High-resolution X-ray powder diffraction data were recorded by a horizontally mounted INEL cylindrical position-sensitive detector (CPS-120) using Debye-Scherrer geometry (angular step ca. 0.029^o-2θ over a 2θ-range from 2 to 115^o) and monochromatic Cu $K\alpha_1$ (λ =1.5406 Å) radiation (40 kV and 25 mA). The system was equipped with a liquid nitrogen 700 series Cryostream Cooler from Oxford Cryosystems possessing an accuracy of 0.1 K. Samples were placed into 0.5-mm-diameter Lindemann capillaries, which were rotating around their axes during data collection to reduce the effects of preferential orientation. The 4096 detector channels were converted to 2θ degrees through a calibration by cubic spline fitting of the diffraction pattern ofthe cubic phase of $Na_2Ca_2Al_2F_4$. The peak positions were determined after pseudo-Voigt fitting of the peaks. Lattice parameters were determined using DICVOL [31] and refined with the FullProf Suite [32] using the LeBail method [33], which does not require any structural model.

The Rietveld analysis of the two hexagonal co-crystals have been analyzed using the FullProf Suite [32]. The C_{60} molecule on Wyckoff site 1a of space group *P6/mmm* has been modeled with spherical harmonics describing a homogeneous distribution of 60 C-atoms positioned on a sphere with a radius of 3.59 Å. The CCl_2Br_2 molecule has been described as a rigid body with the C-atom at the center of the molecule, two Cl-atoms at a distance of 1.77 Å and two Br-atoms at a distance of 1.93 Å. For simplicity the angle between the ligands has been set to that of a perfect tetrahedron. The variable structural parameters within the Rietveld refinement process were the lattice constants, the position of the CCl_2Br_2 molecule and its orientation. An overall isotropic temperature factor has been refined for all involved atoms and the background has been described by a linear interpolation. No symmetry constraint has been assumed for the position of the molecule (Wyckoff site 24r).

3. Results

3.1. The binary system C_{60}-CBr_2Cl_2. Cubic crystals of the solvate C_{60}-CBr_2Cl_2 immediately after removal from the mother liquor can be seen in Fig. 1A.

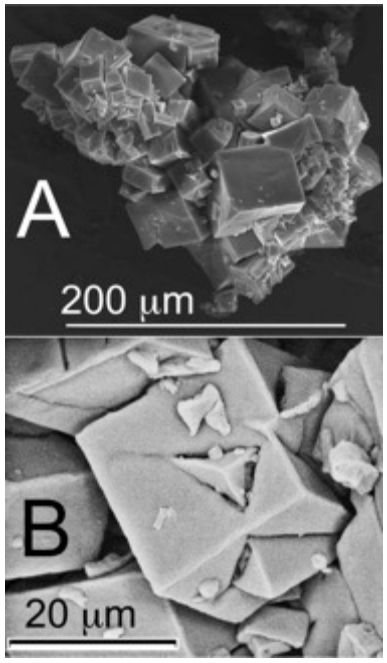

Fig. 1. Scanning electron microscopy photographs of crystals formed by the C_{60}-CBr_2Cl_2 system: **(A)** Cubic crystals of $C_{60}\cdot 12CBr_2Cl_2$ directly obtained from the mother liquor, **(B)** Enlargement of the center of Fig. (A), showing intercalated twinning of the fluorite type with two cubes rotated about [111] [35,36].

Because the cubic co-crystal is not stable in open air, mixtures of the crystals in their mother liquor were placed in stainless steel high-pressure pans for differential scanning calorimetry (DSC) studies. The resulting DSC curve can be seen in Fig. 2B. The endothermic peaks p1 and p2 correspond to transitions of crystalline CBr_2Cl_2: the monoclinic (C2/c) to fcc transition followed by melting of the fcc phase [37]. The onset temperatures are virtually the same as those of pure CBr_2Cl_2; hence, the transitions correspond to degenerated invariant equilibria in the C_{60}-CBr_2Cl_2 binary system. Peaks p3 and p4 in Fig. 2B reflect the peritectic invariants ($L+C_{60}\cdot 12CBr_2Cl_2+ C_{60}\cdot 2CBr_2Cl_2$) and ($L+C_{60}\cdot 2CBr_2Cl_2+C_{60}$), respectively. For verification, X-ray diffraction of cubic crystals with mother liquor in a closed capillary was carried out as a function of temperature. The diffraction patterns confirm the characterization of the different invariants observed in the DSC measurements (see Fig. 2B).

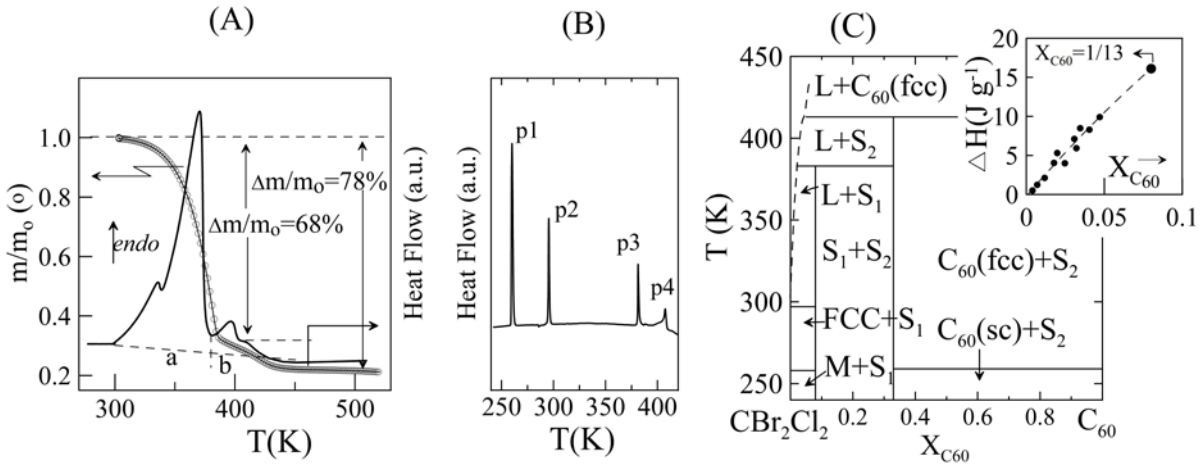

Fig. 2. (A) Thermogravimetric (open circles) and DSC (line) curves for the cubic solvate of $C_{60}\cdot 12CBr_2Cl_2$ in an open pan after the mother liquor had evaporated. **(B)** DSC curve for the cubic crystals in a closed pan demonstrating the monoclinic to fcc transition of CBr_2Cl_2 (p1), melting of CBr_2Cl_2 (p2) and the peritectic invariants $C_{60}\cdot 12CBr_2Cl_2$ + $C_{60}\cdot 2CBr_2Cl_2$ + liquid (p3) and $C_{60}\cdot 2CBr_2Cl_2$ + liquid+C_{60} (p4). **(C)** CBr_2Cl_2 – C_{60} phase diagram. S_1 and S_2 are the respective co-crystals $C_{60}\cdot 12CBr_2Cl_2$ and $C_{60}\cdot 2CBr_2Cl_2$. **Inset:** Tammann diagram for the $C_{60}\cdot 12CBr_2Cl_2$ + $C_{60}\cdot 2CBr_2Cl_2$ + liquid peritectic equilibrium.

Mixtures of cubic crystals in mother liquor were introduced in pierced pans and maintained isothermally at 303 K within the thermogravimetric analyzer to determine the stoichiometry of the solvate. Immediately after the mother liquor had evaporated, the sample was heated to 525 K with a heating rate of 2 K·min^{-1}. The measured mass loss is presented in Fig. 3A and it exhibits two steps over an extensive temperature interval. The final mass loss is about 78%, very near the expected value of 80% for the desolvation process $C_{60}\cdot 12CBr_2Cl_2$ (solid) → C_{60} (solid) + 12 CBr_2Cl_2 (vapor). As for the first step, the mass loss of 68% agrees very well with the transformation from $C_{60}\cdot 12CBr_2Cl_2$ (solid) → $C_{60}\cdot 2CBr_2Cl_2$ (solid) + 10 CBr_2Cl_2 (vapor), i.e., the transformation from cubic to hexagonal co-crystals, with an expected mass loss of 67%.

DSC measurements in pierced pans (Fig. 2A) provide the enthalpy change related to the desolvation process. The complete desolvation enthalpy of the cubic co-crystals, peaks a and b together, equals 124-148 joule per gram of $C_{60}\cdot 12CBr_2Cl_2$ (38-45 kJ/mol of solvent). As for the desolvation of the $C_{60}\cdot 2CBr_2Cl_2$ hexagonal solvate (peak b in Fig. 2A), the desolvation enthalpy is found to be 36-49 joule per gram of solvate (i.e., 22-29 kJ/mol of solvent). Using the experimental stoichiometries and the DSC thermal events, a binary phase diagram of C_{60} and CBr_2Cl_2 can be constructed (Fig. 2C) with the two co-crystals at mole

fractions X=1/13 (C_{60}·12CBr_2Cl_2) and X=1/3 (C_{60}·2CBr_2Cl_2), which, as determined above, possess fcc and hexagonal symmetries, respectively. The enthalpy of the peritectic invariant C_{60}·12CBr_2Cl_2 + C_{60}·2CBr_2Cl_2 + liquid was determined by DSC observing samples with compositions between X=0 (CBr_2Cl_2) and X=1/13 (~0.08, i.e. the C_{60}·12CBr_2Cl_2 co-crystal composition). The enthalpy associated with the peritectic transition at T=382.4 K was found to be 17 joule per gram of cubic co-crystal (see inset of Fig. 2C).

To obtain structural information on these co-crystals, while avoiding loss of solvent molecules, a Lindeman capillary was filled with crystals in the mother liquor for X-ray measurements at room temperature. Diffraction patterns (Fig. 3A) were indexed using DICVOL [31] and a cubic unit cell, presumably $Fm\bar{3}m$ (a=27.884(5) Å, V/Z=2710.1(8) $Å^3$ and Z=8), was found. While the solvent evaporated slowly, hexagonal crystals appeared and the X-ray pattern demonstrated the presence of a new crystal structure (Fig. 3A). After complete evaporation of the solvent, Bragg reflections of the cubic co-crystal have disappeared and they have been replaced by those corresponding to a hexagonal symmetry in line with what is commonly found for solvates of related solvents [22,24,27,34,38]. After pattern indexing and refinement (Fig. 3A), lattice parameters were found to be a =10.1101(8) Å, c= 11.022(9) Å with V=982.7(1) $Å^3$.

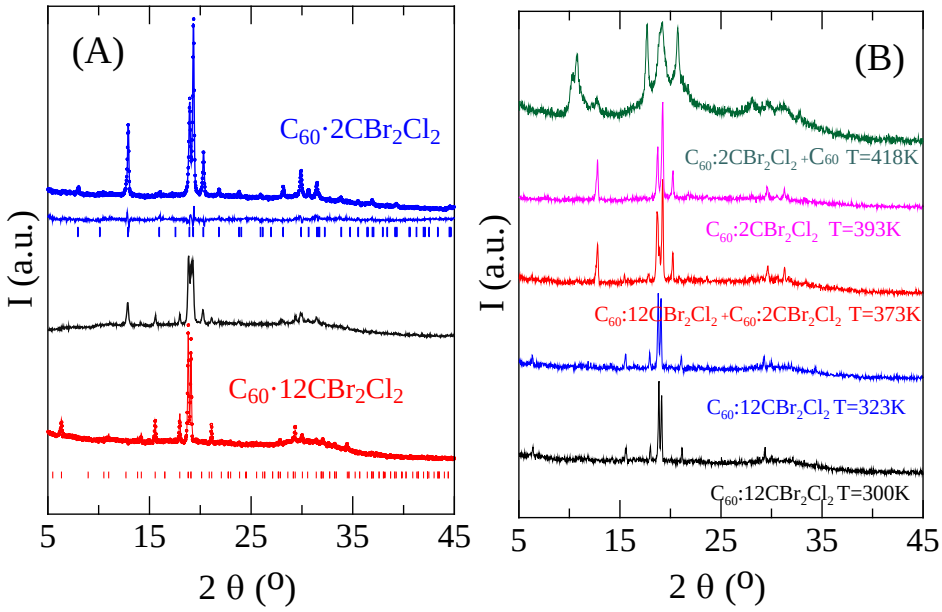

Fig. 3. (A) Experimental (points) and calculated (lines) diffraction patterns along with the calculated Bragg peak positions (vertical bars) for the cubic C_{60}·12CBr_2Cl_2 (red) in the mother liquor and for the hexagonal C_{60}·2CBr_2Cl_2 (blue) solvate. For C_{60}·2CBr_2Cl_2 the

calculated pattern is the result of a Rietveld refinement (the residuals are plotted between the diffraction pattern and the Bragg peak positions), whereas for $C_{60}\cdot 12CBr_2Cl_2$ the calculated pattern has been obtained by the LeBail [33] method (see text). The gray pattern in the center is an intermediate pattern between cubic and hexagonal co-crystals while the mother liquor is evaporating. **(B)** Patterns as a function of temperature from cubic solvate in an excess of mother liquor in a sealed capillary. The range between 45 and 115^o is not shown due to the absence of Bragg peaks with significant intensity. However, the Rietveld refinement included and reproduced the complete pattern.

3.2. The binary system C_{60}-$CBr_2(CH_3)_2$. Cubic crystals were grown at room temperature from a heterogeneous mixture of fcc C_{60} in $CBr_2(CH_3)_2$ in screw-cap flasks, protected from light in the timespan of several weeks. SEM photographs of the crystals are presented in Fig. 4. For X-ray diffraction studies, the crystals were placed in a Lindemann capillary with the mother liquor, because the solvates degraded rapidly when exposed to air. The X-ray pattern (Fig. 5) was indexed using DICVOL resulting in an fcc system and a lattice parameter of a=28.282(3) Å, which, assuming Z=8, gives rise to a lattice volume per molecular unit of V/Z=2827.7 Å^3.

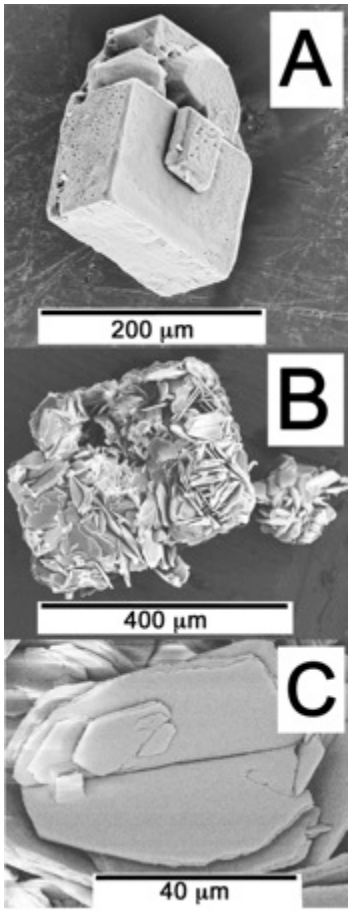

Fig. 4. Scanning electron microscopy photographs of crystals formed by the C_{60}-$CBr_2(CH_3)_2$ system: **(A)** Cubic $C_{60}\cdot 12CBr_2(CH_3)_2$ co-crystals **(B)** Small hexagonal $C_{60}\cdot 2CBr_2(CH_3)_2$ co-crystals grown by heating the cubic co-crystals. **(C)** Detail of photograph B showing the hexagonal plates of $C_{60}\cdot 2CBr_2(CH_3)_2$.

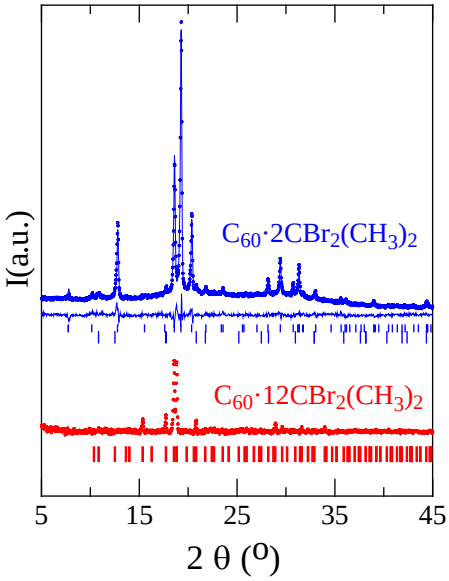

Fig. 5. Experimental (points) and calculated (lines) diffraction patterns along with the calculated Bragg peak positions (vertical bars) for the cubic $C_{60}\cdot 12CBr_2(CH_3)_2$ (red) and for the hexagonal $C_{60}\cdot 2CBr_2(CH_3)_2$ (blue) co-crystals. For $C_{60}\cdot 12CBr_2(CH_3)_2$, the calculated pattern is obtained through the LeBail method (see text), whereas for $C_{60}\cdot 2CBr_2(CH_3)_2$,the calculated pattern is the result of a Rietveld refinement containing 2.9 % of fcc C_{60} (see text) indicated by the longer blue vertical bars among the Bragg peak positions. The residuals between calculated and experimental patterns are plotted between the patterns and the Bragg peak positions. The range between 45 and 115^o is not shown due to the absence of Bragg peaks with significant intensity, however, the Rietveld refinement included and reproduced the entire 2θ range.

The stoichiometry of the cubic co-crystals was determined by measuring the mass loss as a function of time of the crystals in their mother liquor at 303 K. It can be seen in Fig. 6 that first the mother liquor evaporates followed by the desolvation of the cubic co-crystals. The mass loss of the latter process equals 81% counting from point 'a' as indicated in Fig. 6, at which point the mother liquor had fully evaporated. The observed percentage corresponds closely to a 1:12 (C_{60}: $CBr_2(CH_3)_2$) stoichiometry, which is equal to 77%.

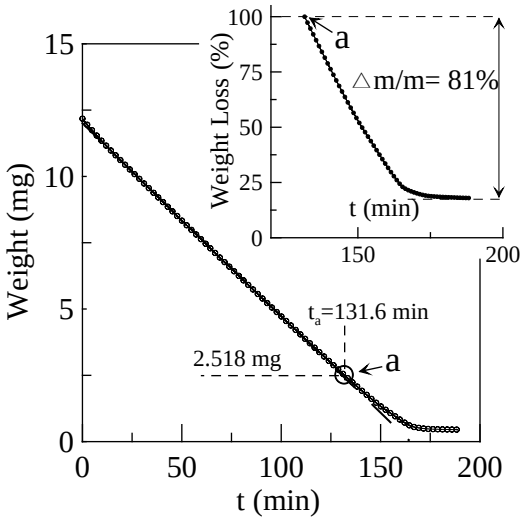

Fig. 6. Isothermal evaporation at 303 K of a sample consisting of cubic co-crystals and mother liquor. The initial segment up to point *a* corresponds to the evaporation of the mother liquor at a rate of 0.072 mg·min^{-1}. For t>t$_a$, spontaneous desolvation of the cubic co-crystals occurs. **Inset:** Close-up of the graph starting at point '*a*', the initial mass of the cubic co-crystals. The mass loss is expressed in % of the initial mass of the co-crystals at t$_a$.

DSC measurements of the cubic crystals together with the mother liquor result in two endothermic peaks (Fig. 7A) corresponding to the degenerate solid-solid phase transition (214.7 K) and fusion (255.0 K) of pure $CBr_2(CH_3)_2$ (peaks p1 and p2, respectively) and an additional endothermic peak at 338.2 K (p3). To investigate which transition was associated to the latter endothermic peak, X-ray diffraction measurements were carried out of crystals in mother liquor in a closed capillary. Fig. 7B reveals that the cubic solvate transforms to crystals with a different symmetry at around 338 K and that at approximately 343 K the latter crystals desolvate and become fcc C_{60}. It is clear that the peritectic equilibrium involving the three phases: cubic co-crystal, a new co-crystal, and the liquid, is very close in temperature to the next peritectic equilibrium between the new co-crystal, fcc C_{60}, and the liquid. To identify the symmetry of the new crystals, several mixtures were heated to about 338 K and then cooled to room temperature. The resulting crystals were examined by SEM and pseudomorphs of the cubic co-crystals partly transformed into hexagonal-shaped plates were observed (see Fig. 4).

Some hexagonal-shaped crystals were subjected to TG, DSC, and X-ray analyses. Fig. 8, presenting the TG and DSC measurements, demonstrates that desolvation of the hexagonal crystals starts around 340 K and accounts for a mass loss of 32%, close to the expected 35.9%

for a 1:2 stoichiometry of $C_{60}\cdot 2CBr_2(CH_3)_2$. The desolvation enthalpy is found to be 60.5 joule per gram of solvate, i.e. 168 joule per gram of solvent (or 34 kJ/mol of solvent).

The X-ray pattern (Fig. 5) was indexed and a hexagonal unit cell was found with lattice parameters a= 10.072(2) Å and c= 11.333(3) Å, which assuming Z=1 results in V/Z=995.6 $Å^3$. The pattern also contains a few Bragg peaks corresponding to fcc C_{60}, most likely due to the proximity of the peritectic equilibrium $C_{60}\cdot 2CBr_2(CH_3)_2 + C_{60}$ + liquid. The presence of fcc C_{60} may also explain the difference between the experimental (32%) and the theoretical (35.9%) mass loss.

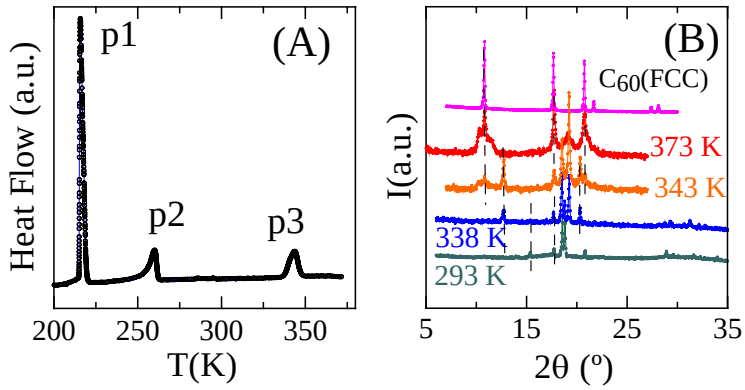

Fig. 7. (A) DSC curve obtained in a sealed pan of cubic solvate of $C_{60}\cdot 12CBr_2(CH_3)_2$ in the presence of mother liquor. The solid-solid transition (p1) and melting (p2) of $CBr_2(CH_3)_2$ can be observed as well as a peak consisting of the convoluted peritectic invariants $C_{60}\cdot 12CBr_2(CH_3)_2 + C_{60}\cdot 2CBr_2(CH_3)_2$ + liquid and $C_{60}\cdot 2CBr_2(CH_3)_2$ + liquid + C_{60} (p3). (B) X-ray diffraction patterns of the cubic solvate in mother liquor in a closed capillary as a function of temperature, 293 K: cubic solvate ($C_{60}\cdot 12CBr_2(CH_3)_2$) + liquid (mother liquor); 338 K: cubic solvate ($C_{60}\cdot 12CBr_2(CH_3)_2$) and hexagonal solvate ($C_{60}\cdot 2CBr_2(CH_3)_2$) + liquid; 343 K: hexagonal solvate ($C_{60}\cdot 2CBr_2(CH_3)_2$) and fcc C_{60} + liquid; 373 K: fcc C_{60} + liquid. The pattern on top is that of fcc C_{60} and is provided for reference.

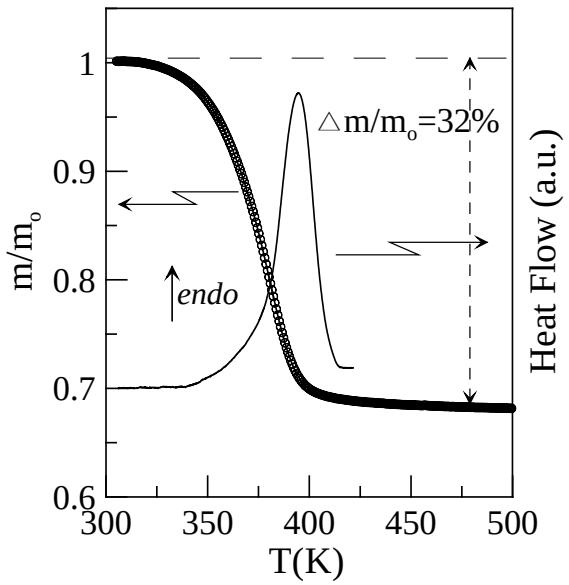

Fig. 8. TG and DSC desolvation measurements of the hexagonal solvate $C_{60}\cdot 2CBr_2(CH_3)_2$.

3.3. Structural characterization of the hexagonal solvates

Because the cell metrics are very similar to those of chloroform solvates of fullerenes [39] the starting positions of the C_{60} and the guest molecules for the refinement process have been chosen accordingly. However, different starting orientations of the guest molecules have been tested in order to avoid convergence in a local minimum. The result of the refinement (Fig. 3 for X-ray patterns and Fig. 9 for the structure) demonstrates that the CCl_2Br_2 molecule is situated approximately at the prismatic hexagonal void with the refined position of [0.377(4), 0.689(4), 0.507(4)] (Note that the position of the guest molecule refers to the position of the central C atom). The distance to the position (1/3, 2/3, 1/2) is 0.5 Å, which may be due to the fact that the center of mass of the molecule does not coincide with the central C-atom. The refined angles do not reveal any special orientation of the molecule with respect to the high symmetry directions of the unit cell resulting in a rather spherical distribution of the Br- and Cl-atoms, when dynamic disorder is taken into account. The starting orientation did not have an influence on the result of the Rietveld refinement, i.e. the final orientations were always symmetry equivalent which corroborates the validity of our result. The refined lattice constants are a=10.09(1) Å and c=11.10(1) Å. The agreement factors are R=14.9 and χ^2=1.55. Very similar results have been obtained for the $CBr_2(CH_3)_2$ solvate. This molecule too was simplified to a perfect tetrahedron with bond lengths C-Br=1.95 Å and C-C=1.53 Å taken from reference [41]. Because of their low X-ray contrast, the H-atoms of the methyl groups have been neglected in the description of the rigid body

molecule. The position of the central C-atom was refined to [0.358(4), 0.633(2), 0.519(2)] being at a distance of 0.47 Å from the prismatic hexagonal void. The lattice parameters are a=10.07(1) Å and c=11.40(1) Å (R=11.3, χ^2=1.82). The fcc C_{60} phase is present in the solvates, as demonstrated by a some weak peaks in the diffraction pattern (see Fig. 5). The Rietveld refinement yields a volume fraction of less than 2.9(2)%.

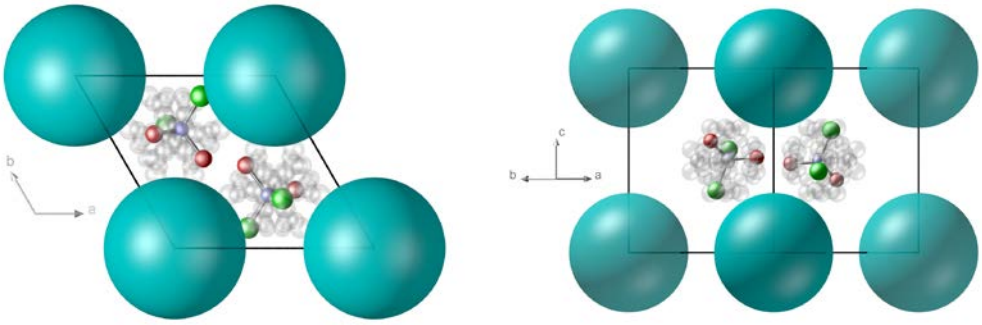

Fig. 9. Structure of the C_{60}·2 CCl_2Br_2 hexagonal solvate along [001] (left) and [110] (right) directions. The orientational disorder of the CCl_2Br_2 molecules at the prismatic positions is highlighted by several compatible orientations in grey.

4. Discussion

The excess volume of a crystal is defined by $\Delta V/V=[(V/Z)^{exp}-(V/Z)^{cal}]/(V/Z)^{cal}$, where $(V/Z)^{exp}$ and $(V/Z)^{cal}$ are the experimental and calculated volumes of the crystal lattice per molecular unit. The excess values of the cubic and hexagonal solvates have been calculated using the molecular volumes from the literature for C_{60} (V_{C60}=710Å^3/molecule), CBr_2Cl_2($V_{CBr2Cl2}$=162.03Å^3/molecule) for the high-temperature fcc phase [41] and $CBr_2(CH_3)_2$ ($V_{CBr2(CH3)2}$ = 165.2 Å^3/molecule) according to the available density values [30]. The excess volumes for the cubic solvates, which are not stable in air, were found to be positive: C_{60}·12CBr_2Cl_2 has a ΔV/V of +2% and C_{60}·12$CBr_2(CH_3)_2$ has an excess volume of +5% similar to the positive excess volumes of cubic C_{60} solvates reported in previous studies [24,25,26,28]. Negative values were found for the hexagonal solvates, that appear to be more stable in air: the ΔV/V of C_{60}·2CBr_2Cl_2 equals -5% and that of C_{60}·2$CBr_2(CH_3)_2$ is -4.3%.

Fig. 10A shows the volume per molecular unit (Z') in the hexagonal solvates as a function of the van-der-Waals volume of the solvent molecules calculated with Kitagorodskii's approach [41]. The linear trend demonstrates that the lattice volume of

hexagonal solvates is governed by molecular size, the larger the guest molecule, the larger is the unit cell of the co-crystal. The result is independent of the dipole moment of the guest molecule as can be inferred from the fact that they range from 0.2 D (for CBr_2Cl_2 and $CBrCl_3$) to 2.11 D (for $CCl_3(CH_3)$) [37.42,43]. The inset of Fig. 10A demonstrates that the same seems to be true for the reduced number of cubic solvates obtained in this work as well as reported previously in the literature [22]. They all correspond to the stoichiometry 1:12 for the C_{60}/solvent ratio.

Intermolecular interactions can also be related to the packing coefficient $\kappa = V_{vdw}/(V/Z)$, which is defined as the ratio between the sum of the van-der-Waals molecular volumes of the individual molecules, V_{vdw}, and the unit-cell volume V divided by Z, the number of molecular entities in the unit cell. Hence the van-der-Waals volume for the C_{60} solvates is: $V_{vdw}=aV_{vdw}(solvent)+V_{vdw}(C_{60})$, where 'a' is 12 or 2. The resulting packing coefficients have been plotted in Fig. 10B as a function of the van-der-Waals volumes of the single solvent molecules. For the hexagonal solvates, two different trends are observed. For solvates containing solvent molecules with C_{3v} (CCl_3Br, $CCl_3(CH_3)$), C_{2v} (CBr_2Cl_2 or $CBr_2(CH_3)_2$) and higher symmetry (as CCl_4 with T_d symmetry), but without an H-atom bound to the central carbon, the packing coefficients increase linearly. However, they are much lower than packing coefficients of solvates possessing an H-atom attached to the central carbon atom. It implies that the molecules CCl_3H, CBr_3H, and CBr_2ClH fit better in the interstitial sites between the layers of C_{60} molecules in the *a*-*b* planes along the *c* axis. It has been shown previously [23] that the solvent molecules fill the prismatic hexagonal voids in the primitive hexagonal packing of the solvates (space group P6/mmm). It has been demonstrated that for the CCl_3H and CBr_3H molecules a three-fold disorder exists [23]. Thus, taking the molecules in Fig. 10B with a three-fold molecular symmetry axis CCl_3H, CBr_3H, and CBr_2ClH (assuming disorder with respect to the halogen atoms) and an H-atom bonded to the central carbon atom, the more efficient packing can be explained by placing their three-fold axis, i.e. the C-H bond, parallel to the *c* axis of the hexagonal unit cell. This is supported by the observed C_{60}-C_{60} distances in the (*00l*) hexagonal planes. Fig. 11 depicts the hexagonal lattice parameters as a function of the van-der-Waals volume of single solvent molecules. A clear anisotropy of the hexagonal lattice exists for the [001] planes and (*001*) direction. The C_{60}-C_{60} distances in the [001] planes, i.e. the a lattice parameter, are virtually constant irrespective of the solvent volume (the average hexagonal lattice parameter is 10.14±0.05 Å for all analyzed solvates), whereas the hexagonal lattice strongly increases along the ***c*** direction depending on the solvent; however, this effect is almost absent for the solvates with

the C-H three-fold symmetry axis (including CBr_2ClH). Any increase in the lattice parameter a as a function of the van-der-Waals volume is most likely due to disorder around the C-H three-fold axis. For the other solvent molecules, the disorder appears to extend over all four positions, explaining the increase of the lattice parameter c with the solvent size.

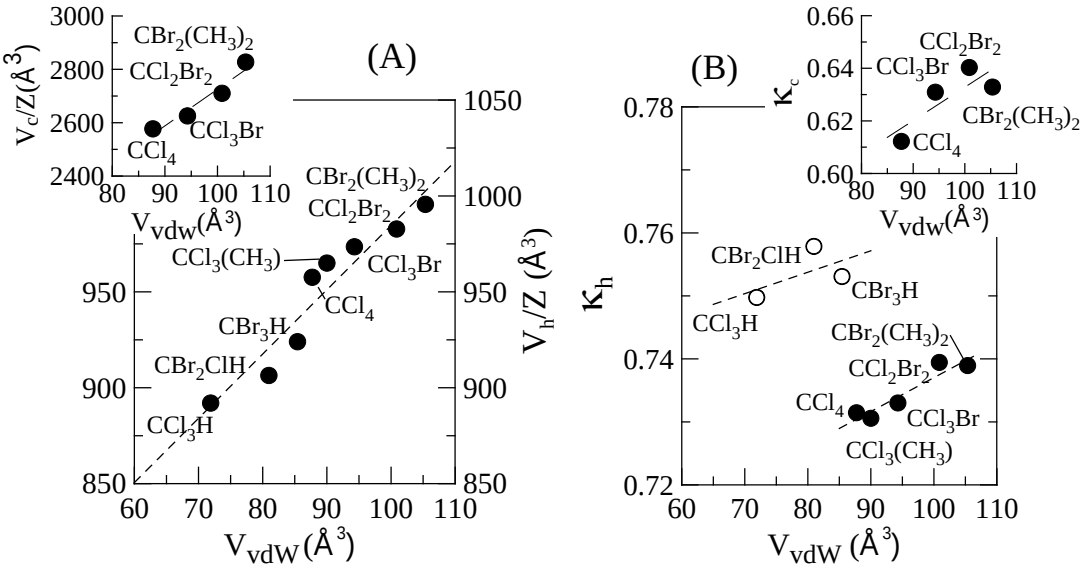

Fig. 10. (A) Volume of the hexagonal solvate per molecular unit (Z') and **(B)** packing coefficient as a function of the van-der-Waals volumes of a single solvent molecule. **Insets:** the same graphs for the cubic solvates, which are not stable in air.

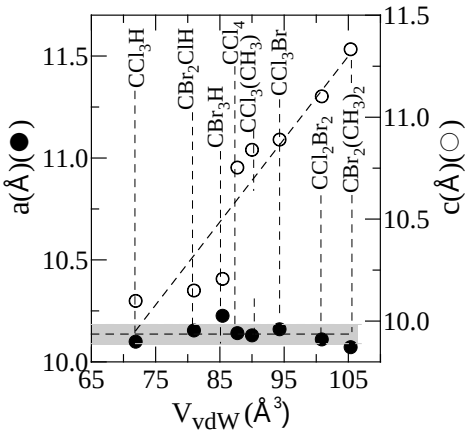

Fig. 11. Hexagonal lattice parameters a (solid circles) and c (open circles) as a function of the van-der-Waals molecular volumes of the solvents.

5. Conclusions

The solvates $C_{60}\cdot 2CBr_2Cl_2$ and $C_{60}\cdot 2CBr_2(CH_3)_2$, stable in open air, possess a hexagonal structure (space group P6/mmm), as revealed by X-ray diffraction. The solvent molecules are positioned close to the prismatic hexagonal voids between the fullerene C_{60} molecules and they are orientationally disordered. The hexagonal solvates possess negative excess volumes (-5% and -4.3% for $C_{60}\cdot 2CBr_2Cl_2$ and $C_{60}\cdot 2CBr_2(CH_3)_2$, respectively), whereas the cubic solvates, which are not stable in open air, have positive excess volumes (+2% and +5% for $C_{60}\cdot 12CBr_2Cl_2$ and $C_{60}\cdot 12CBr_2(CH_3)_2$, respectively). The excess volumes correlate with the relative stabilities of the solvates.

A comparison with previously reported C_{60} solvates reveals that the unit-cell volumes of the hexagonal solvates increase with the size of the guest molecule, which in first instance may appear rather straightforward. However, taking the molecular symmetry into account, it has been shown that for molecules with a three-fold symmetry axis around a C-H bond, the axis is found to be parallel to the *c* hexagonal axis, increasing the packing efficiency along this direction. Solvent molecules that lack the hydrogen atom attached to the central carbon atom exhibit disorder over all four atoms covalently bonded to the central atom, which explains the linear increase of the hexagonal *c* axis with solvent size.

Supporting Information

Crystallographic information files for $C_{60}\cdot 2CBr_2Cl_2$ (C60-2CBr2Cl2_RT.cif) and $C_{60}\cdot 2CBr_2(CH_3)_2$ (C60-2CBrMe2_RT.cif) hexagonal co-crystals at room temperature.

Conflict of interest

The authors declare no competing financial interests**.**

Graphical Abstract

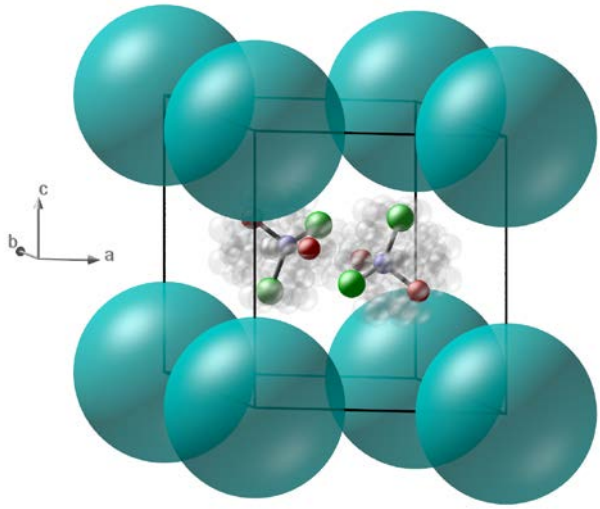

ACKNOWLEDGEMENTS

The authors thank Dr I. López (Departmentof Materials and Metallurgic Engineering, UPC) for his assistance with the SEM experiments. This work has been supported by the Spanish MEC (FIS2014-54734-P) and by the Catalan government (2014SGR-00581).

REFERENCES

[1] Y. Iwasa, K. Tanoue, T. Mitani, A. Izuoka, T. Sugawara, T. Yagi, Chem. Commun. 13 (1998) 1411.

[2] R. Macovez, M. R. C. Hunt, J. A. Shan, Th. Goldoni, M. Pichler, P. Pedio, Moras, C. Castellarin-Cudia, J. Schiessling, L. Venema, P. Rudolf, New. J. Phys. 11 (2009) 023035.

[3] A. L. Briseno, S. C. B. Mannsfeld, M. M. Ling, S. H. Liu, R. J. Tseng, C. Reese, M. E. Roberts, Y. Yang, F. Wudl, Z. N. Bao, Nature. 444 (2006) 913.

[4] W. Ma, C. Yang, X. Gong, K. Lee, A. J. Heeger, Adv. Funct. Mater. 15 (2005) 1617.

[5] S. Cho, J. H. Seo, K. Lee, A. J. Heeger, Adv. Funct. Mater. 19 (2009) 1459.

[6] L. D. Zheng, Y. Han, J. Phys. Chem. 116 (2012) 1598.

[7] M. V. Korobov, A. L. Mirakian, N. V. Avramenko, E. F. Valeev, I. S. Neretin, Y. L.; Smith,A. L. Lovokhotov, G. Olofsson, R. S. Ruoff, J. Phys. Chem. B. 102 (1998) 3712.

[8] M. Akada, T. Hirai, J. Takeuchi, T. Yamamoto, R. Kumashiro, K. Tanigaki, Phys. Rev. B. 73 (2006) 094509.

[9] H. Takeya, K. Miyazawa, R. Kato, T. Wakahara, T. Ozaki, H. Okazaki, Y. Takano, Molecules. 17 (2012) 4851.

[10] P.R. Somani, S.P. Somani, M. Umeno, Appl. Phys. Lett. 91 2007 173503.

[11] F. Yang, S. R. Forrest, Anodes. Adv. Mater. 18 (2006) 2018.

[12] K. Ogawa, T. Kato, A. Ikegami, H. Tsuji, N. Aoki, Y. Ochiai, J. P. Bird, Appl. Phys. Lett. 88 (2007) 112109.

[13] R. Colle, G. Grosso, A. Ronzani, M. Gazzano, V. Palermo, Carbon. 50 (2012) 1332.

[14] M. T. Rispens, A. Meetsma, R. Rittberger, C. J. Brabec, N. S. Sariciftci, J. C. Hummelen, Chem. Comm. 17 (2003) 2116.

[15] L. J. Wang, Phys. Chem. Solids. 84 (2015) 85.

[16] K. N. Semenov, N. A. Charykov, V. A. Keskinov, A. K. Piartman, A. A. Blokhin, A. A. Kopyrin, J. Chem. Eng. 55 (2010) 13.

[17] C. Smart, B. Eldridge, W. Reuter, J. A. Zimmerman, W.R. Creasy, N. Rivera, R. S. Ruoff, Chem. Phys. Lett. 188 (1992) 171.

[18] M. V. Korobov, E. B. Stukalin, A. L. Mirakyan, I. S. Neretin, Y. L. Slovokhotov, A. V. Dzyabchenko, A. I. Ancharov, B. P. Tolochko, Carbon. 41 (2003) 2743.

[19] A.V. Dzyabchenko, V. Agafonov, V. A. Davydov, J. Phys. Chem. A 103 (1999) 2812.

[20] L. Wang, B. Liu, H. Li, W. Yang, Y. Ding, S. V. Sinogeikin, M. Yue, Z. Liu, X. C. Zeng, W. L. Mao, Science 337 (2012) 825.

[21] V. D. Blank, S. G. Buga, M. Y. Popov, V. A. Davidov, H. Szwarc, A. Rassat, G. Fabre, New. J. Chem. 19 (1995) 253.

[22] R. Céolin, D. O. López, B. Nicolaï, P. Espeau, M. Barrio, H. Allouchi, J. Ll. Tamarit, Chem. Phys. 342 (2007) 78.

[23] R. E. Dinnebier, O. Gunnarsson, H. Brumm, E. Koch, A. Huq, P. W. Stephens, M. Jansen, Science. 296 (2002) 109.

[24] R. Céolin, J. Ll. Tamarit, M. Barrio, D. O. López, P. Espeau, H. Allouchi, R. J. Papoular, Carbon. 43 (2005) 417.

[25] M. Barrio, D. O. López, J. Ll. Tamarit, P. Espeau, R. Céolin, Chem. Mater. 15 (2003) 288.

[26] B. Keita, L. Nadjo, R. Céolin, V. Agafonov, D. Andre, H. Szwarc, J. Dugue, C. Fabre, A. Rassat, Chem. Phys. Lett.179 (1994) 595.

[27] R. Céolin, J. Ll. Tamarit, M. Barrio, D. O. López, S. Toscani, H. Allouchi, V. Agafonov, H. Szwarc, Chem. Mater. 13 (2001) 1349.

[28] M. Barrio, D. O. López, J. Ll. Tamarit, H. Szwarc, S. Toscani, R. Céolin, Chem. Phys. Lett. 260 (1996) 78.

[29] R. Windiks, A. Bill, B. Delley, V. Z. Kresin, Phys.Rev. B. 66 (2002) 195418.

[30] A. Würflinger, L. C. Pardo, Naturfors. 57a (2002) 177.

[31] A. Boultif, D. Louer, J. Appl. Cryst. 37 (2004) 724.

[32] C. J. Rodriguez, T. Roisnel, P. J. Gonzales, FullProf suite (2005 version). CEA-CNRS, CEN Saclay, France: Laboratoire Léon Brillouin.

[33] A. LeBail, Powder Diffraction 20 (2005) 316.

[34] P. Espeau, M. Barrio, D. O. López, J. Ll. Tamarit, R. Céolin, H. Allouchi, V. Agafonov, F. Masin, H. Szwarc, Chem. Mater. 14 (2002) 321.

[35] C. Giacovazzo, Fundamentals of Crystallography 2nd Ed. IUCr – Oxford Science publications, 2002.

[36] U. Müller, Symmetry Relationships Between Crystal Structures, Oxford University Press, 2013.

[37] M. Barrio, J. Ll. Tamarit, P. Negrier, L.C. Pardo, N. Veglio, D. Mondieig, New. J. Chem. 32 (2008) 232.

[38] C. Collins, J. Foulkes, A. D. Bond, J. Klinowski, Phys. Chem. Chem. Phys.1 (1999) 5323.

[39] L. A. Solovyov, N. V. Bulina, G. N. Churilov, Russ. Chem. Bull. 50 (2001) 78.

[40] Ph. Negrier, M. Barrio, J. Ll. Tamarit, N. Veglio, D. Mondieig, Cryst. Growth & Des. 10 (2010) 2793.

[41] A. Kitaigorodskii, Organic Chemical Crystallography; Consultants Bureau: New York, 1961.

[42] L. C. Pardo, M. Barrio, J. Ll. Tamarit, D. O. López, J. Salud, H. A. J. Oonk, Chem. Mater. 17 (2005) 6146.

[43] B. Parat, L. C. Pardo, M. Barrio, J. Ll. Tamarit, P. Negrier, J. Salud, D. O. López, D. Mondieig, Chem. Mater. 17 (2005) 3359.